# A novel fault diagnosis technique for photovoltaic systems based on artificial neural networks

W. Chine [a], A. Mellit [a, b], V. Lughi [c], A. Malek [d], G. Sulligoi [c], A. Massi Pavan [c, *]

[a] Renewable Energy Laboratory, Faculty of Sciences and Technology, Department of Electronics, University of Jijel, Ouled-Aissa, P.O. Box .98, Jijel, 18000, Algeria
[b] The Abdus Salam International Centre for Theoretical Physics (ICTP), Strada Costiera, 11, 34151, Trieste, Italy
[c] Department of Engineering and Architecture, University of Trieste, Via A. Valerio, 6/A, 34127 Trieste, Italy
[d] Centre de Développement des Energies Renouvelables BP. 62 Route de l'Observatoire, Bouzareah 16340 Alger, Algeria

ARTICLE INFO

Accepted 6 January 2016

*Keywords:*
photovoltaics
Fault detection
Fault diagnosis
ANN
FPGA

ABSTRACT

This work proposes a novel fault diagnostic technique for photovoltaic systems based on Artificial Neural Networks (ANN). For a given set of working conditions - solar irradiance and photovoltaic (PV) module's temperature - a number of attributes such as current, voltage, and number of peaks in the current –voltage (I–V) characteristics of the PV strings are calculated using a simulation model. The simulated attributes are then compared with the ones obtained from the field measurements, leading to the identification of possible faulty operating conditions. Two different algorithms are then developed in order to isolate and identify eight different types of faults. The method has been validated using an experimental database of climatic and electrical parameters from a PV string installed at the Renewable Energy Laboratory (REL) of the University of Jijel (Algeria). The obtained results show that the proposed technique can accurately detect and classify the different faults occurring in a PV array. This work also shows the implementation of the developed method into a Field Programmable Gate Array (FPGA) using a Xilinx System Generator (XSG) and an Integrated Software Environment (ISE).

## 1. Introduction

Over the past few years, the number of photovoltaic (PV) systems has increased rapidly at the global level. Grid-connected PV plants with size varying from a few kWp (domestic systems) to hundreds of MWp (commercial/industrial and utility-scale systems) represent worldwide the power technology with the highest growth rate. As reported in Refs. [1], at the end of 2014 the total installed PV capacity was 177GWp. This result is not only related to the incentives given by governments during the past years but also to the recent attainment of the grid-parity in key countries such as Germany and Italy [2,3].

The need for higher performance, efficiency, and reliability is linked to the recent interest in fault diagnosis techniques that are today more and more proposed in the literature. A remote monitoring and fault detection method, which relies on a satellite-based systems to generate the necessary climate data at the desired location, is presented in Ref. [4]. The proposed technique leads to the detection of four different categories of failures. 1) Constant energy losses due, for example, to the degradation of PV modules, to the soiling effect, to PV module or string failures, etc. 2) Variable energy losses due, for example, to shading phenomena [5], to soiling effects [6–8], to mismatch effects [9–11], to disconnections of the PV system from the electrical grid, to inverter's power limitation, to Maximum Power Point Tracker (MPPT) failures, to the temperature effect, etc. 3) Losses due to the presence of snow. 4) Losses due to blackouts [12]. The proposed technique leads to a reduction of the computational and simulation costs but, on the other hand, the costs for data loggers and communication systems are high. Nowadays, as the overnight capital cost of PV plants has dramatically decreased, the development of cheap monitoring systems is necessary.

A monitoring circuit measuring the operating voltage ($V_{mpp}$) and current ($I_{mpp}$), the open circuit voltage ($V_{oc}$), and the short circuit current ($I_{sc}$) of PV modules is proposed in Ref. [13]. The circuit can detect the shadow propagation along a PV string, the number of shaded subpanels, as well as the efficiency of the MPPT. In Refs. [14], the authors proposed a low-cost on-board monitoring device that

* Corresponding author.
*E-mail address:* apavan@units.it (A. Massi Pavan).

improves the system's reliability and efficiency. The method takes as an input the measure of the PV panel's current, voltage, and temperature. A novel technique for the transmission of the current, voltage, and temperature quantities based on a low cost smart monitoring system is proposed in Ref. [15]. A data acquisition board sends the data to a central control system using the Power Line Carriers (PLC) communications technology, avoiding additional installations costs.

In general, fault detection methods for PV systems can be grouped as visual (browning, discolouration, surface soiling, and delamination), thermal (hot spot), and electrical (transmittance line diagnosis, dark/illuminated current–voltage measurement, and RF measurement) [16]. In this paper we focus on an electrical method. Fault detection based electrical methods for photovoltaic systems are based on:

- Methods that do not require climate data (such as solar irradiance and temperatures): in Ref. [17] the authors developed a method based on the Earth Capacitance Measurement (ECM) to detect the disconnection of a PV module. The Time-Domain Reflectometry (TDR) technique proposed in Ref. [18] was used to detect the disconnection of a PV string as well as the impedance change due to degradation. In Refs. [19], a statistical approach based on the Analysis of Variance (ANOVA) and on the non-parametric Kruskale Wallis (KW) tests was investigated;
- Methods based on the analysis of the current voltage characteristic (I–V characteristic): in Refs. [20], the (dI/dV) - V characteristic is used to detect the partial shadow interesting a PV array. In Refs. [21], the authors calculate the Fill Factor (FF), the series resistance (Rs), and the shunt resistance (Rsh) starting from the I–V characteristic and provide some performance indicators. A method based on the evaluation of some current and voltage indicators is introduced in Ref. [22] as automatic fault detection for Grid-Connected Photovoltaic (GCPV) systems;
- Methods that use a Maximum Power Point Tracking (MPPT) approach: an automatic supervision and fault detection procedure based on the analysis of the power losses was proposed in Ref. [23]. The method leads to the identification of three groups of faults (faulty module, faulty string, and a group of different faults such as partial shadow, ageing, and MPPT failure) and of a false alarm. The method presented in Ref. [24] detects faults occurring in both the PV array and in the inverter on the base of a power losses analysis. The technique developed in Ref. [25] is based on the relation between the simulated and the measured string powers. This method determines the number of open and short-circuited PV modules in a string;
- Methods based on Artificial Intelligence (AI) techniques: a learning method based on Expert Systems is developed in Ref. [26] to identify two types of fault (due to the shading effect and to the inverter's failure). The effectiveness of Artificial Neural Network (ANN) based techniques was shown in Ref. [27]. A method for the identification of short-circuited PV modules is presented in Ref. [28]. In Refs. [29], an ANN is used in order to classify different types of faults occurring in a PV array. In this case, the ANN takes as inputs the current and the voltage at maximum power point, and the temperature of the PV module. Different methods based on the Takagie Sugeno Kahn Fuzzy Rule (TSKFRBS) have been described in Refs. [30,31].

Other strategies comprise: a method based on the extended correlation function and on the matter element model was presented in Ref. [32]. In Refs. [33], a Decision Tree (DT) technique was used to examine two different types of faults using an Over-Current Protection Device (OCPD). The first type of fault is the line-to-line fault that occurs under low irradiance conditions, and the second is the line-to-line fault occurring in PV arrays equipped with blocking-diodes [34]. An equivalent circuit model was proposed in Refs. [35] and [36] for the calculation of the PV generator's insulation resistance and leakage current. This model can be used to analyse the risk of electric shock and for the design of protections. Sources of failure and PV modules diagnostics are reviewed in Ref. [37].

The main contribution of this work is to present a new technique for the isolation and identification of the faults occurring in a PV system and its implementation into a FPGA. In particular, the technique is able to localize and identify faults occurring in: PV cells, PV modules, PV strings, and bypass-diodes. The proposed technique is based on the analysis of a set of attributes (such as current, voltage and number of peaks) of the I–V characteristic that indicate the normal and the faulty operations. The analysis is performed using two different Algorithms:

- Algorithm 1 implements a signal threshold approach and isolates the faults that have a different combination of attributes;
- Algorithm 2 consists of an ANN-based approach to identify the faults that are characterized by the same combination of attributes.

The paper is organized as follows: the next section presents the main types of faults occurring in a PV array. The proposed fault diagnosis technique is provided in Section 3. Results and discussion are given in Section 4.

## 2. Faults in photovoltaic arrays

The faults occurring in a PV system are mainly related to the PV array, the inverter, the storage system, and the electrical grid. This work aims at detecting the faults occurring in the PV array and, with reference to Table 1, eight different faults are investigated. This type of faults are usually connected to: the failure of a solar cell or a PV module, a line disconnection, the degradation effect, corrosion and manufacturing defects, the presence of snow, the effect of soiling, and etc.

## 3. The proposed fault diagnosis technique

The fault diagnosis technique developed in this work is able to identify one normal and eight faulty modes. As shown in Fig. 1, firstly the difference between the measured and the simulated PV array output power is compared with a threshold (*Th*) in order to detect the possible presence of a fault. Then, the analysis of the main attributes in the I–V characteristic of each string forming the PV array leads to the faults identification and localization. The schematic of the developed fault diagnosis system that is based on two different Algorithms, is depicted in Fig. 2.

### 3.1. Attributes identification

In order to understand what changes can affect the attributes of an I–V characteristic, a number of simulations have been carried out considering both normal operation and different fault conditions. The simulations have been performed using a MatLab/Simscape™ tool. As an example, Fig. 3a shows the Simscape™ based model for a PV string formed by four series-connected modules, in case of connection fault [38]. Standard blocks representing the PV modules, resistances, current and voltage sensors have been used. A PV module block consists of four series-connected PV modules, and these are made by 18 series-connected solar cells as depicted in Fig. 3b. The solar cell block is defined by equation (1) [39] [40], where Iph is the photo-generated current, I0 is the dark saturation

**Table 1**
Different type of faults occurring in a PV array.

| Types of fault | Name | Symbol |
|---|---|---|
| Module | Short circuit fault in any bypass diode or (cell or module) | F1 |
| | Inversed bypass diode fault or (cell or module) | F2 |
| | Shunted bypass diode fault or (cell or module) | F3 |
| | Open circuit fault in any cell or (module) | F4 |
| Connection fault | Connection resistance between PV modules | F5 |
| Partial shadow fault | Shadow effect in the modules with normal operation of different components of PV string | F6 |
| Shadow effect with faulty by pass diode | Shadow effect in a group of cells equipped by a faulted bypass diode open | F7 |
| Shadow effect with connection fault | Shadow effect in a group of module connected by a connected resistance | F8 |

current, Rs is the module series resistance, Rsh is the module shunt resistance, a is the diode ideality factor, K is Boltzmann's constant, and q is the charge of the electron. The five parameters (Iph, I0, Rs, Rsh, a) are determined by solving the transcendental equation (Eq. (1)) using the Newton Raphson algorithm based only on the data-sheet of PV module [40]. These five parameters as well as the solar irradiance are inserted in the block parameters of the solar cell, as shown in Fig. 3c, in order to simulate the I–V characteristic.

$$I = I_{ph} - I_0\left(e^{q\left(\frac{V+I\,R_s}{K\,T}\right)} - 1\right) - \left(\frac{V + IR_s}{R_{sh}}\right) \quad (1)$$

Fig. 4a–b presents the I–V characteristics of the PV string for normal and faulty conditions at the same operating conditions. The analysis of these simulations led to the identification of the following situations:

- A reduction in the short circuit current (C1);
- A reduction in the open circuit voltage (V1);
- A reduction or an increase in the output current (C2);
- A reduction or an increase in the output voltage (V2);
- An increased number of MPPs in the I–V characteristic (N).

### 3.2. Attributes combination

The combination of the changes in the attributes can be related to both the number and type of faults and to the change in the operating conditions. As an example, Table 2 reports different possible combinations, here after also named *fault signature*, of attributes.

Table 2 Reveals that a fault may be characterized by more than one fault signature and also that different faults can have the same combination of attributes. As an example, the first signature of F3 and F5, and the second signature of F2 and F3 present the same fault signature.

Nevertheless, Table 3 shows that different faults always lead to different attributes, even if they present the same signature.

The faults are then classified into two groups:

- Faults characterized by the same fault signature. This type of faults are isolated using a signal threshold based approach;
- Faults with different fault signatures. These faults are isolated using an ANN-based approach.

#### 3.2.1. Signal threshold based approach (Algorithm 1)

The first algorithm isolates the faults when these have a different combination of attributes. First, the measured and simulated PV strings attributes are calculated and the relative differences are compared with some thresholds. The simulated I–V characteristics come from a reference model [37] based on the values of solar irradiance and module's temperature and specifications.

The thresholds are calculated on the basis of the maximum error

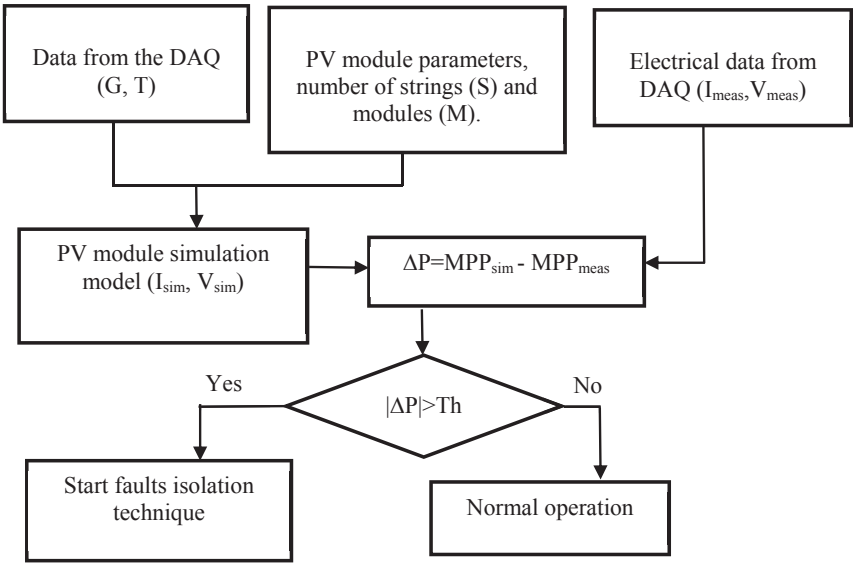


**Fig. 1.** Block diagram of the proposed fault detection technique.

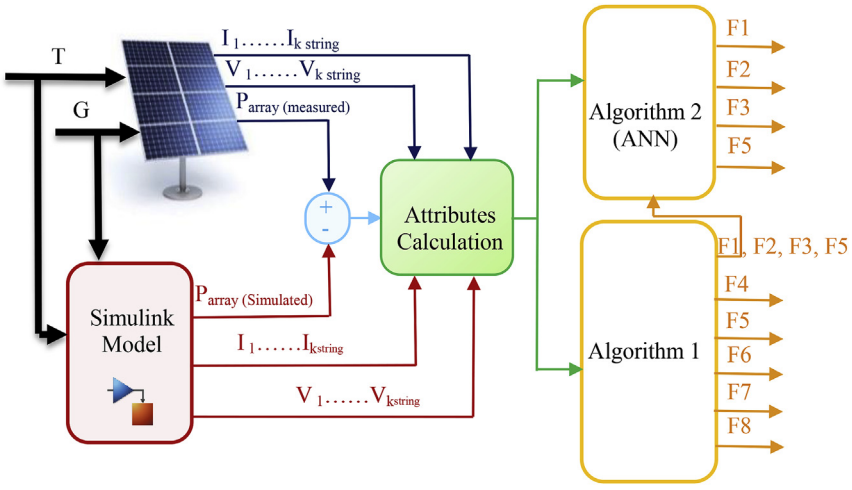


**Fig. 2.** Schematic of the proposed fault diagnosis technique.

introduced by the model uncertainty and the measurement noise. The sensors used to validate the proposed diagnostic system are within the specifications required by the IEC 61724 standard [41] that indicates a relative error of 1%, 1%, and 2% while measuring current, voltage, and power, respectively. The model uncertainty is related to the manufacturing tolerance and sensors noise. The maximum error introduced by this uncertainty is calculated, according to [42], by adding a dispersion parameter to the simulation model parameters. The obtained relative errors associated to current, voltage, and power are equal to 3.0%, 2.9%, and 5.9%, respectively.

Fig. 5 shows the flowchart of Algorithm 1 that allows the isolation of the following six different situations:

✓ Module open circuited: F4;
✓ Connection fault: F5;
✓ Partial shadow (bypass diodes work correctly): F6;
✓ Partial shadow (when a bypass diode is faulted): F7;
✓ Partial shadow with connection fault: F8;
✓ A group of faults including: F1, F2, F3, and F5.

*3.2.2. ANN based approach (Algorithm 2)*

With reference to Fig. 5, the first algorithm cannot distinguish the faults F1, F2, F3, and F4, as these latter have the same signatures; on the other hand the symptoms of the I–V characteristic under these faults have different amplitudes at the same climatic condition. Thus, in other to isolate these faults, a classification technique was needed, and an ANN technique has been choose.

The ANN model has been developed as follows:

- Selection of input and output variables;
- Data set normalization;
- Selection of network structure;
- Network training;
- Network test.

A data set of 775 patterns has been generated using a MatLab/Simscape™ simulation tool. The 80% of the patterns has been used for the training, while 20% has been used for testing the model.

In order to select the most efficient architecture for the ANN, a comparison between two architectures widely utilized for the classification of faults has been performed: the Multilayer Perceptron (MLP) and the Radial basis function (RBF).

The MLP architecture consists of three neurons in the input layer corresponding to the ratio between the measured and the simulated values of the open circuit voltage (Rvoc), the maximum power point current (Rimpp), and the maximum power point voltage (Rvmpp). One neuron in the output layer corresponds to the fault class. The number of hidden layers and the number of neurons in each layer are determined during the training process; the transfer function used in this layer is the logarithmic sigmoidal function. The network is trained with the Levenberg–Marquardt (LM) algorithm.

The RBF architecture consists of three layers. The input layer has as many neurons as the MLP network, the output layer has four neurons corresponding to the four fault classes, and the hidden layer consists of M neurons. Each neuron computes a Kernel function which is usually a Gaussian function, specified by its center and width; these two parameters are determined by a K-means clustering algorithm, while the weights between the middle layer and the output layer are calculated with a pseudo inverse matrix method.

## 4. Results and discussion

This section reports the results of the Simscape™ based model as well as the performances of the proposed fault diagnosis technique. The implementation into a Field Programmable Gate Array (FPGA) is also presented. For the online localization and identification of faults, the proposed technique requires a reference solar cell, a PV module's temperature sensor, a current and a voltage sensor. The data are collected by a data acquisition system and transferred to a personal computer where the routine for the diagnostic procedure is implemented.

*4.1. Experimental results*

The model used to simulate the I–V characteristics for the different faults conditions has been experimentally validated using the data from a PV string installed on the rooftop of the REL at Jijel University (Algeria). The string consists of four series-connected Polycrystalline Silicon PV modules with a nominal power of 120Wp. The modules are made of 72 series-connected solar cells, while groups of 18 cells are equipped with a bypass diode [43].

The experimental set up with the different faults configurations

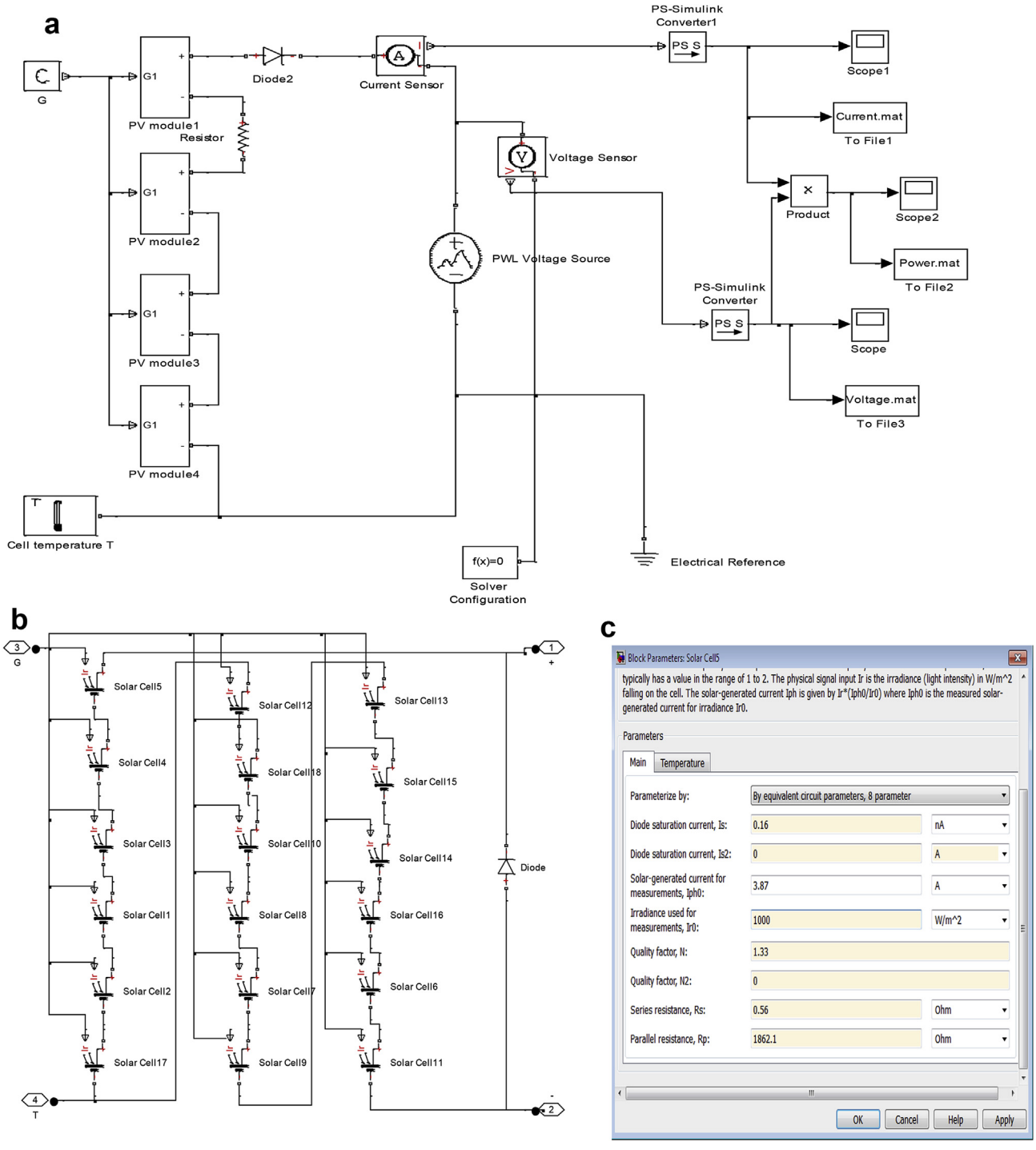


**Fig. 3.** (a)The Simscape™ model: case of a connection fault occurring in a PV string. (b). 18 solar cells in series connected. (c). Block parameters of solar cell.

and the test facility are shown in Fig. 6a–f, g–h,and 7, respectively.

As an example, Fig. 8a–d shows the simulated and the experimental I–V characteristics corresponding to different fault conditions.

As can be seen, a good agreement between measured and simulated data is achieved. The relative errors are in the following ranges:

- short circuit current [1.1–1.6%];
- output current [1.5–4.7%];
- open circuit voltage [1.0–2.0%];
- output voltage [1.1–3.8%].

Fig. 8ashows that the short circuit current and the open circuit voltage decrease when a bypass diode is shunted or inversed; in this latter case, the phenomenon is more evident. When a bypass diode is short-circuited, there is only a decrease in the open circuit voltage while the short circuit current remains the same.

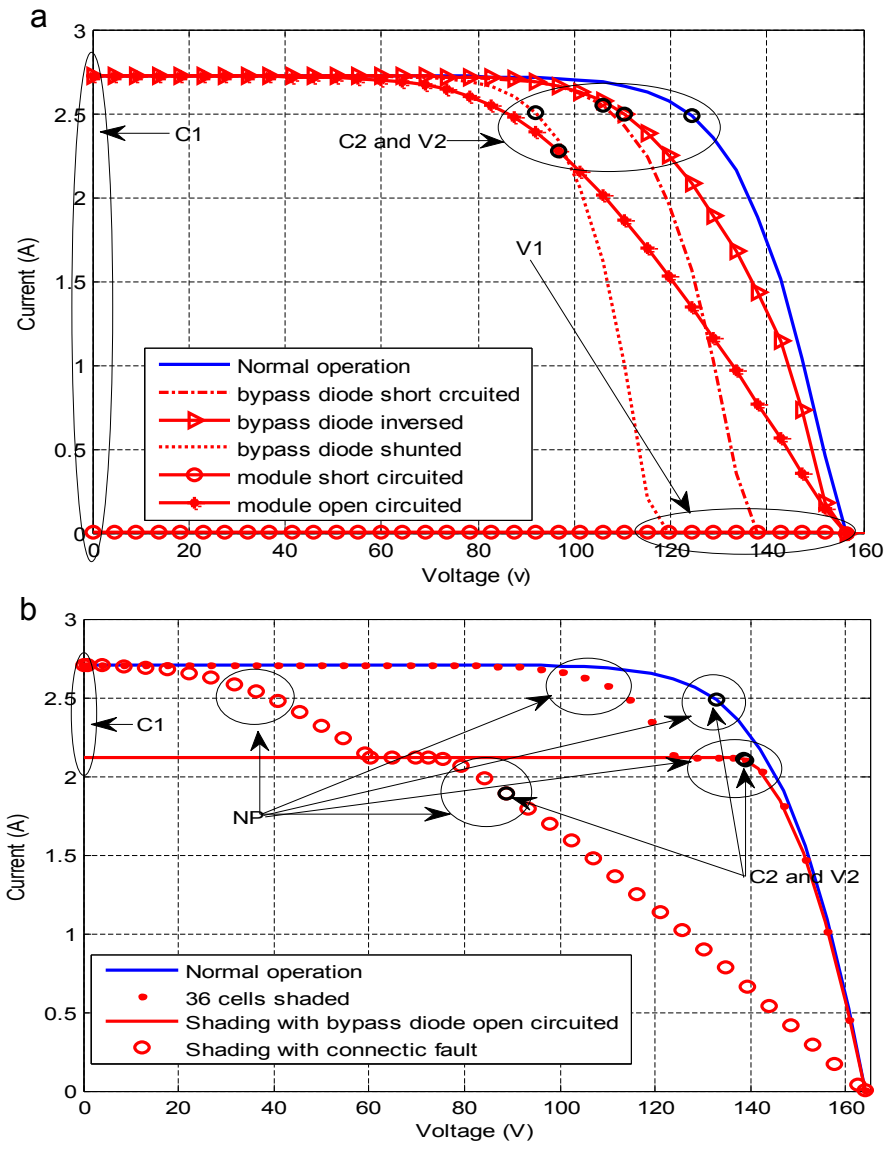


**Fig. 4.** (a). I–V characteristics of a PV string for normal and faulty operations without shading effect. (b). I–V characteristics of a PV string for normal and faulty operations with shading effect.

As shown in Fig. 8b, a fault in a PV module leads to a decrease of both the open circuit voltage and the short circuit current; the open circuit voltage drop is more evident when the PV module in inversed. The open circuit voltage varies very slightly in the case of a connection fault, while the short circuit current decreases (Fig. 8c).

Finally, Fig. 8d shows that in the case of shading the open circuit voltage decreases only when a bypass diode is inversed, while the short circuit current always decreases.

### *4.2. Performance evaluation of the proposed technique*

#### *4.2.1. Performance evaluation of Algorithm 1*

In order to verify the performance of Algorithm 1, a PV array formed by two strings of nine series-connected PV modules has been considered, and three case studies have been examined in case of STC:

- Case 1: one module was 50% shaded and equipped with four open-circuited bypass diodes;
- Case 2: two modules were shaded (the shading factor was 50% for the first module and 75% for the second);
- Case 3: The connection resistance between two modules was increased by 15Ω;

The calculated attributes are reported in Table 4.

The STC power of the considered PV array is 1072.2 W, the STC short circuit current is 3.87A, and the STC open circuit voltage is 383.6 V. The thresholds used when comparing the measured and the simulated quantities has thus been calculated as follow:

- Th = 2 × 1072.2 x (2% + 5.9%) = 169.4 W;
- T1 = 3.87 × (3% + 1%) = 0.25 A;
- T2 = 383.6 × (2.9% + 1%) = 14.96 V.

As reported in Table 4, the attributes which exceed the

**Table 2**
Combination of attributes for different faults cases.

| | String output Current | String output Voltage | String short Circuit current | String open Circuit voltage | Number of MPP |
|---|---|---|---|---|---|
| F1 | No change | Decreased | No change | Decreased | 1 |
| F2 | No change | Decreased | No change | Decreased | 1 |
| | No change | Decreased | No change | Decreased | 1 |
| F3 | Decreased | Decreased | No change | Decreased | 1 |
| | No change | Decresead | No change | No change | 1 |
| F4 | Decreased | Decreased | Decreased | Decreased | 1 |
| F5 | No change | Decreased | No change | No change | 1 |
| | Decreased | Decreased | No change | No change | 1 |
| | No change | Decreased | No change | Decreased | >1 |
| F6 | Decreased | Increased | No change | Decreased | >1 |
| | Decreased | No change | No change | Decreased | >1 |
| | Decreased | Increased | No change | No change | >1 |
| | Decreased | Increased | Decreased | No change | 1 |
| F7 | Decreased | Increased | Decreased | Decreased | 1 |
| | Decreased | No change | Decreased | Decreased | 1 |
| | Decreased | Decreased | Decreased | Decreased | 1 |
| | No change | Decreased | No change | Decreased | 1 |
| | Decreased | Decreased | No change | Decreased | 1 |
| | Decreased | Decreased | No change | Decreased | >1 |
| F8 | Decreased | Decreased | No change | No change | >1 |
| | Decreased | Decreased | Decreased | Decreased | >1 |
| | Decreased | Decreased | Decreased | No change | >1 |

**Table 3**
Attributes for two different case studies (Operating conditions: G = 700W/m$^2$, T = 25 °C).

| | $I_{mpp}$ (A) | $V_{mpp}$ (V) | $I_{sc}$ (A) | $V_{oc}$ (V) | Number of MPP |
|---|---|---|---|---|---|
| Case 1 | No change | Decreased | No change | No change | 1 |
| F3 | 2.4537 | 119.808 | 2.709 | 165.888 | 1 |
| F5 | 2.44 | 101.37 | 2.709 | 165.888 | 1 |
| Case 2 | No change | Decreased | No change | Decreased | 1 |
| F2 | 2.5 | 101.37 | 2.709 | 129.024 | 1 |
| F3 | 2.44 | 105 | 2.709 | 161.28 | 1 |
| No fault | 2.4672 | 133.632 | 2.709 | 165.888 | 1 |

predetermined thresholds have been indicated in bold. The obtained results show that the algorithm is able to localize and identify correctly the faults in the examined PV array.

#### 4.2.2. Performance evaluation of Algorithm 2

The adopted ANN structures have been developed after a number of experiments, and with reference to Fig. 9a–b the PMC structure consists of two hidden layers and 13 × 13 hidden nodes. The minimum Mean Square Errors (MSE) achieved during the training and test processes are 0.008 and 0.009, respectively. The

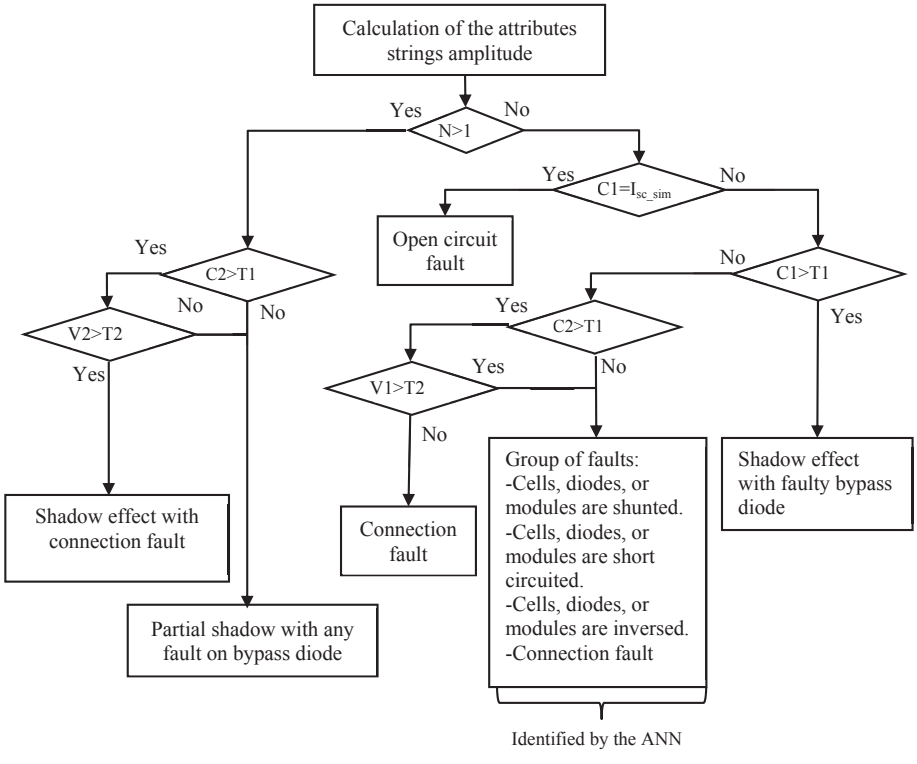


**Fig. 5.** The proposed fault isolation technique.

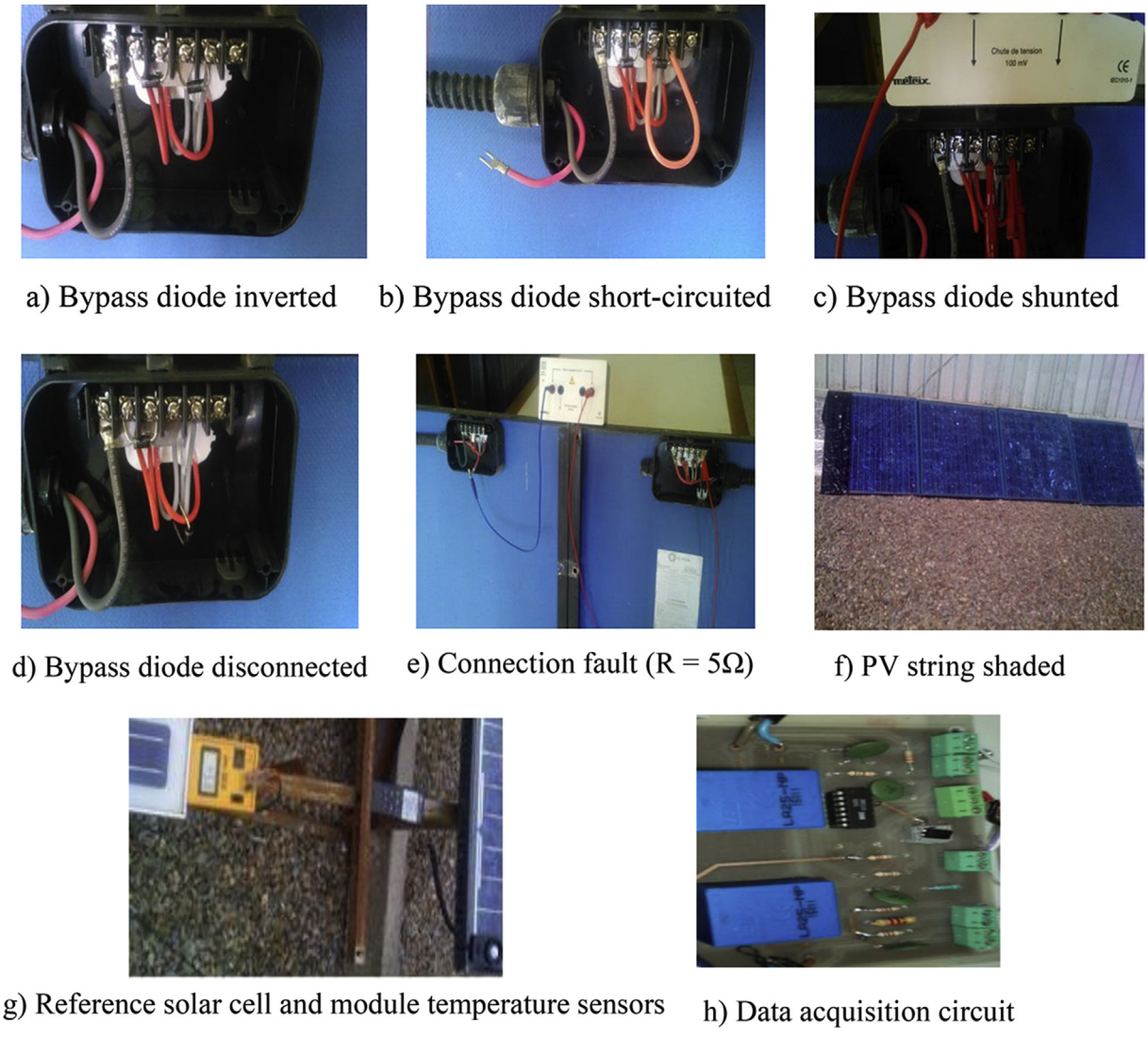


**Fig. 6.** Experimental set up.

RBF structure consists of 49 hidden nodes, and the minimum MSEs achieved during the training and test processes are 0.05 and 0.12 respectively. In order to analyse the effectiveness of the proposed ANN-based approaches, Fig. 10a–b shows the classification confusion matrix for the four faults considered during the test phase. The cells of the matrix with red and green colours represent the percentage of faults correctly and not correctly classified, respectively.

**Fig. 7.** Test facilities at the REL, Jijel University (Algeria).

The classification confusion matrix reveals that the correct and the false classification rates obtained with the MLP based model are 90.3% and 9.7%, respectively. False classifications occurred between F1 and F2, and between F3 and F5. The 28.2% of samples associated to F2 are classified as F1 and this situation occurred when the number of inversed cells or bypass diodes was very low. Furthermore, the 10.5% of samples associated to F5 are classified as F3; this occurred when the connected and shunt resistances had either a very low or a very high values, respectively. Consequently, the power loss was not important in either of the two cases. For the RBF based model, the correct and the false classification rates are 68.4% and 31.6%, respectively, the false classification rate of each class is as follow: 85% for class 1, 6.5% for class 2, 27.5% for class 3, and 61.9% for class 4. The comparison between the results shows that the MLP network is more efficient for faults classification with respect to the RBF one.

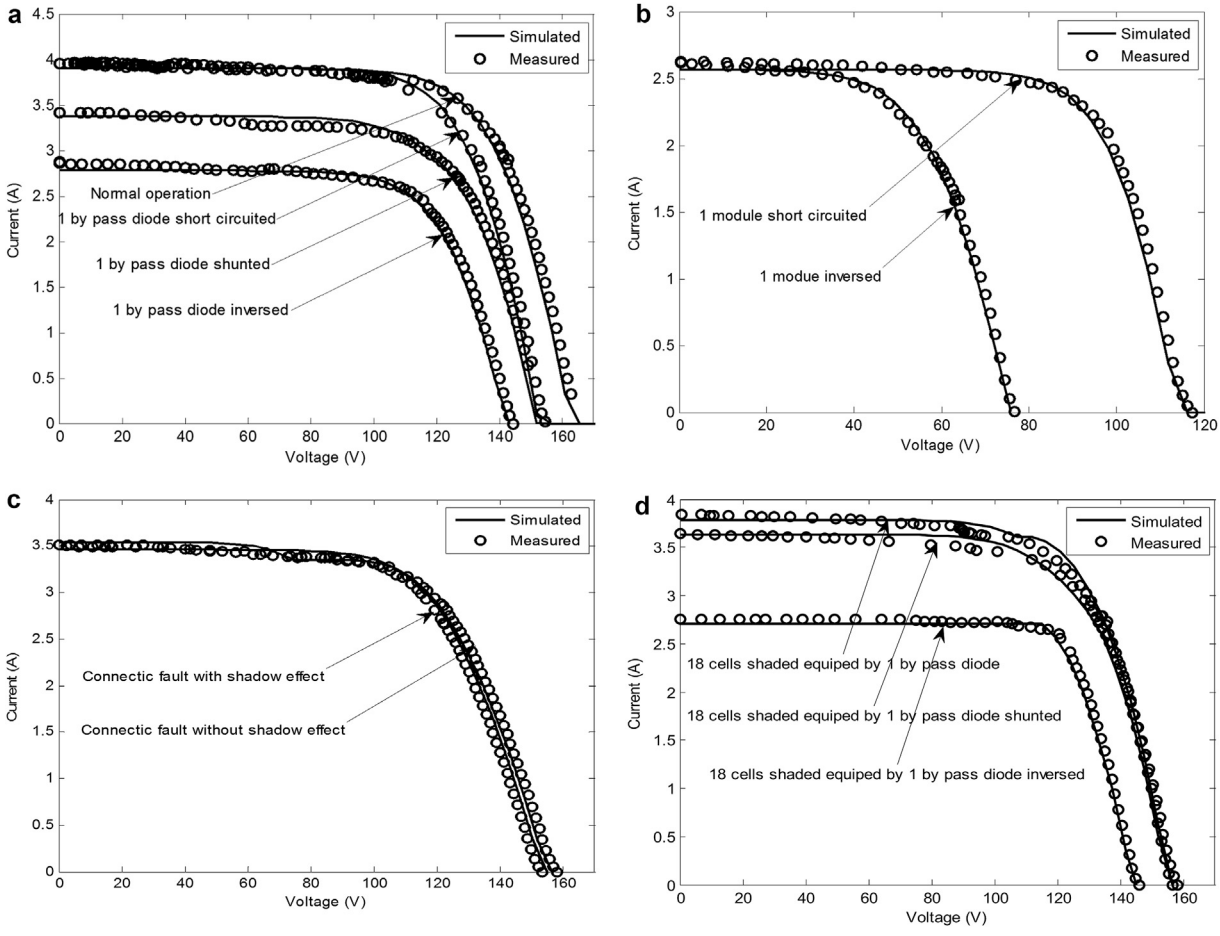


**Fig. 8.** (a). PV string I–V characteristics: case of bypass diode fault. (b). PV string I–V characteristics: case of PV module fault. (c). PV string I–V characteristics: case of connection fault. (d). PV string I–V characteristics: case of shadow effect and possible bypass diode fault.

**Table 4**
Attributes for the considered case studies.

| Case | ΔP | C1 | C2 | V1 | V2 | ΔN |
|---|---|---|---|---|---|---|
| 1 | **369.6** | **1.75** | **1.46** | **20.7** | **31.1** | 0 |
| 2 | **267.1** | 0 | 0.036 | 0 | **72.6** | **2** |
| 3 | **187.3** | 0 | 0.15 | 0 | **41.5** | 0 |

### 4.3. Comparative study

In order to test the effectiveness of the proposed diagnostic method, we have compared the obtained results with the ones from the method presented in Ref. [23]. The comparison between the outputs given by the two methods is presented in Table 5 for four different case studies. As can be noticed, the power losses analysis method only gives the possible fault locations and cannot identify the possible fault types.

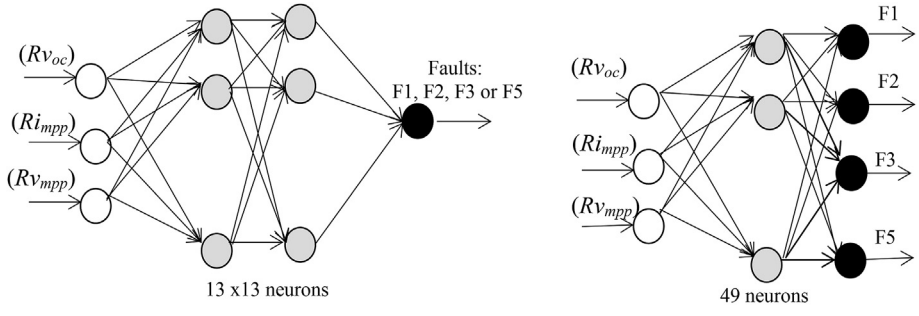


**Fig. 9.** The adopted ANN architecture.

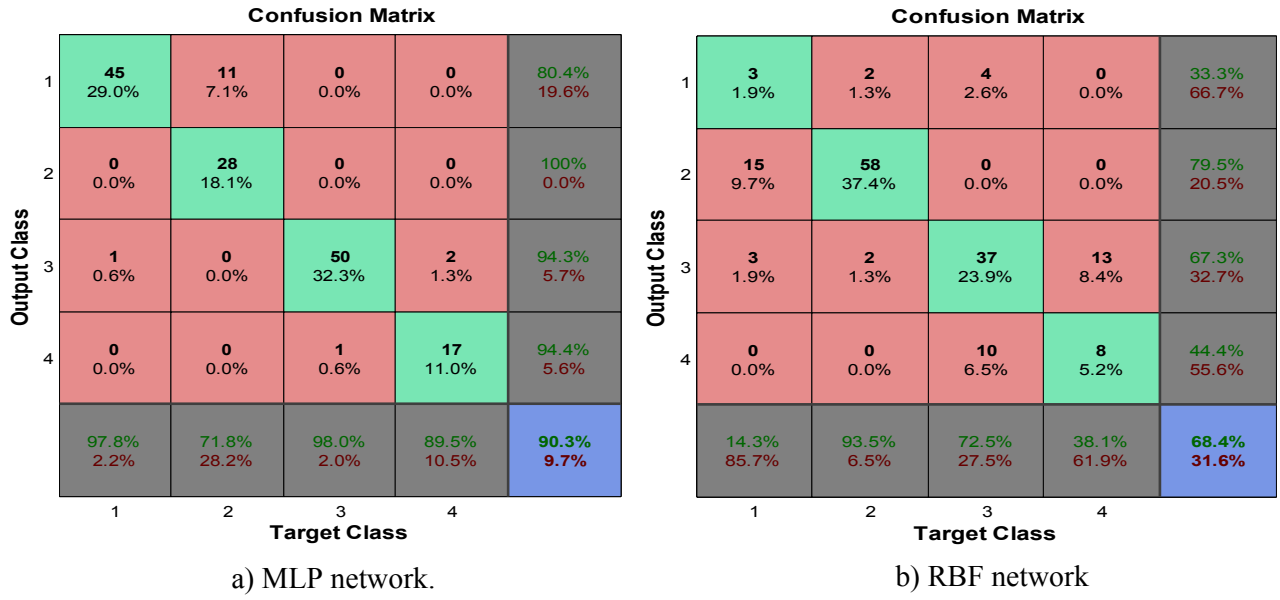


a) MLP network. b) RBF network

**Fig. 10.** Classification confusion matrix for ANN network.

**Table 5**
Comparative results between the proposed method and the one presented in Ref. [23].

| Case study | Method based on power losses analysis | | Proposed method | |
|---|---|---|---|---|
| | Method parameters | Decision method | Method parameters | Decision method |
| String with two shaded modules | $L_{C\_sim} = 0.0037$, $L_{C\_meas} = 0.18$, $\sigma = 0.05$, $R_I = 1$, $R_V = 1.33$ | Faulty module | *ALgorithm1*: N = 2, C2 = 0.01, T1 = 0.1 | Partial shadow with any fault on bypass diode |
| String with two shaded modules equipped by open circuit diodes | $L_{C\_sim} = 0.0037$, $L_{C\_meas} = 0.39$, $\sigma = 0.05$, $R_I = 2.7$, $R_V = 0.88$ | Faulty string | *Algorithm1*: N = 1, C1 = 1.6, T1 = 0.1 | Partial shadow with faulty bypass diode |
| String with two short circuit modules | $L_{C\_sim} = 0.0037$, $L_{C\_meas} = 0.16$, $R_I = 1.01$, $R_V = 1.27$, $\sigma = 0.05$ | Faulty module | *Algorithm 1*: N = 1, C1 = 0.02, C2 = 0.03, T1 = 0.1<br>*Algorithm 2*: $RV_{oc} = 0.5$ $RV_{mpp} = 0.48$ $RI_{mpp} = 0.97$ | Group of faults not discriminable<br>Cells, diodes, or modules are short circuited. |
| String with two shunted modules | $L_{C\_sim} = 0.0037$, $L_{C\_meas} = 0.15$, $R_I = 1.03$, $R_V = 1.22$, $\sigma = 0.05$ | Faulty module | *Agorithm1*: N = 1, C1 = 0.01, C2 = 0.4, T1 = 0.1,V1 = 13.8, T2 = 11.4<br>*Algorithm 2*: $RV_{oc} = 0.95$, $RV_{mpp} = 0.72$, $RI_{mpp} = 0.82$ | Group of faults not discriminable<br>Cells, diodes, or modules are shunted |

$L_{C\_sim}$: simulated capture losses, $L_{C\_sim}$: measured capture losses, $R_{I:}$ current ratio, $R_V$: voltage ratio, $\sigma$: threshold.

### 4.4. FPGA-based implementation

For a rapid prototyping, the designed fault diagnosis technique has been implemented into a FPGA using a Xilinx's System Generator (XSG) with an ISE Ver. 14.3 Design Suite [44]. Fig. 11a shows the proposed method in the FPGA environment. As an example, Fig. 11b depicts the XSG design of Algorithm 1, while Fig. 11c presents the XSG design of the basic elements of the developed ANNs [45]. The hardware co-simulation using the ISE (synthetize and routing) creates automatically the bit stream file and programs the FPGA (type Virtex 5ML501-XC5VLX50).

## 5. Conclusions

The paper presents a new Artificial Neural Network (ANN) based approach for the identification of eight types of fault occurring in a PV array. Moreover, this work also shows the implementation of the proposed fault diagnosis technique into a Field Programmable Gate Array (FPGA) showing its effectiveness in real applications. Different attributes (such as current, voltage and number of peaks) of the simulated and the measured current–voltage (I–V) characteristics of a number of PV strings have firstly been compared. The development of two different algorithms allows the isolation and the identification of faults that have and have not the same combination of attributes. The model used for the simulations of normal and faulty conditions has been experimentally validated using the data from a PV string installed on the rooftop of the Renewable Energy Laboratory (REL) at the Jijel University (Algeria). The obtained results confirm the ability of the technique to correctly localize and identify the different type of faults.

The designed diagnostic method, that can easily be generalized for large-scale PV systems, is cheap as requires as an input only the

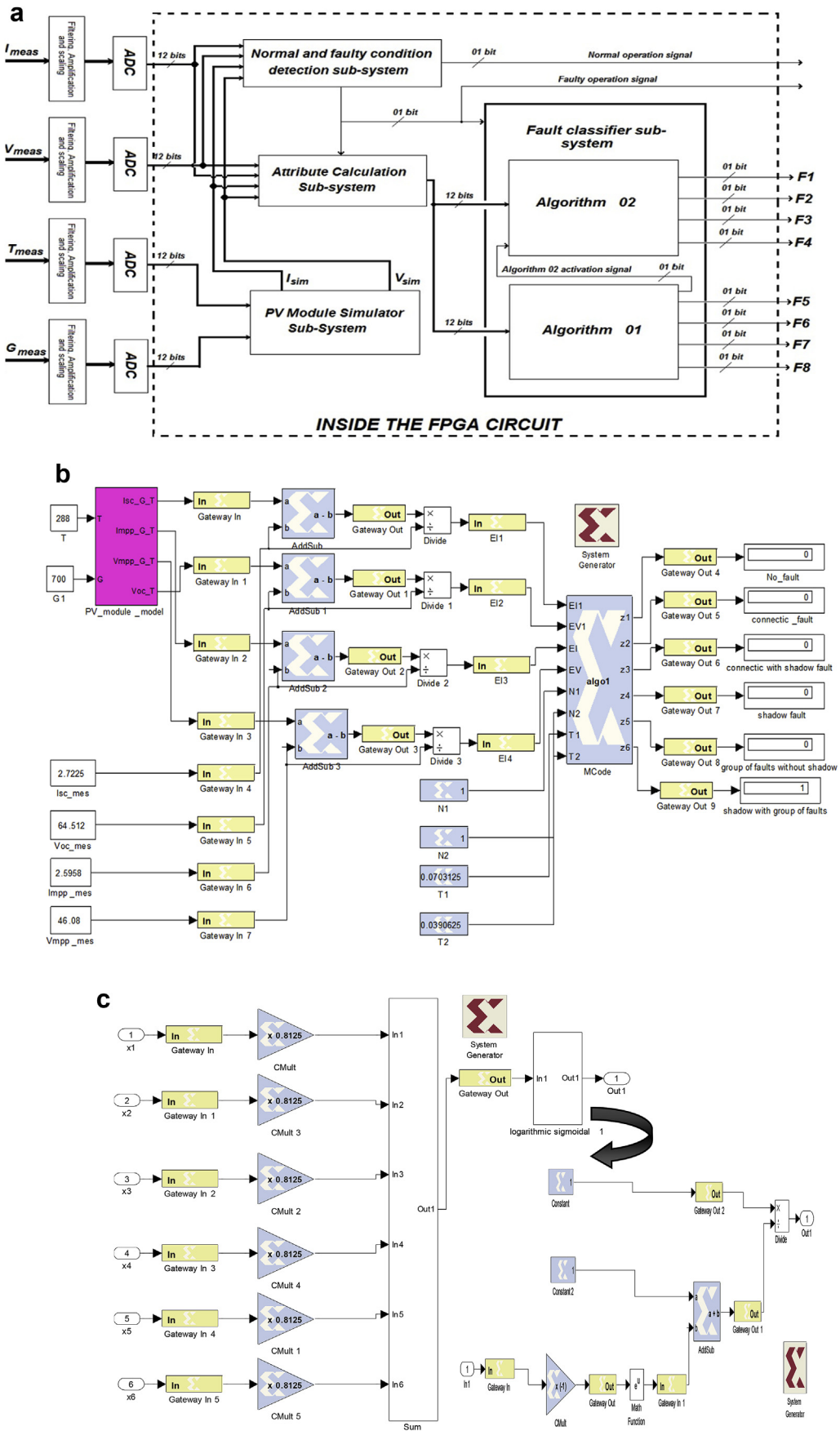


**Fig. 11.** (a)The fault diagnosis configuration using a FPGA environment. (b). XSG design of Algorithm 1. (c). XSG design of the basic elements of Algorithm 2.

following parameters: solar irradiance, PV module's temperature, and PV array's current and voltage. Further investigation aims at experimentally verifying the implemented algorithms into a reconfigurable FPGA for online fault detection and classification.

## Acknowledgements

This work was partially supported by the TWAS under grant (Ref 12-194RG/REN/AF/AC_C: UNESCO FR: 3240270869) and the German Academic Exchange Service (DAAD 09752002). The second author expresses a special acknowledgement to the International Centre for Theoretical Physics (ICTP), Trieste, Italy.

## References

[1] IEA, A Snapshot of Global Markets, Report IEA-PVPS T1 26, 2015.
[2] A. Massi Pavan, V. Lughi, Grid parity in the Italian commercial and industrial electricity market, in: IEEE International Conference on Clean Electrical Power, Alghero (Italy), 2014, pp. 332–335.
[3] A. Massi Pavan, V. Lughi, Photovoltaics in Italy: toward grid parity in the residential electricity market, in: IEEE International Conference on Microelectronics, Algiers (Algeria), 2012, pp. 1–4.
[4] A. Drews, A.C. de Keizer, H.G. Beyer, E. Lorenz, J. Betcke, W. van Sark, Monitoring and remote failure detection of grid-connected PV systems based on satellite observations, Sol. Energy 81 (2007) 548–564.
[5] M. Drif, A. Mellit, J. Aguilera, P.J. Pérez, A comprehensive method for estimating energy losses due to shading of GC-BIPV systems using monitoring data, Sol. Energy 86 (2012) 2397–2404.
[6] A. Massi Pavan, A. Mellit, D. De Pieri, The effect of soiling on energy production for large-scale photovoltaic plants, Sol. Energy 85 (2011) 1128–1136.
[7] A. Massi Pavan, A. Mellit, D. De Pieri, S.A. Kalogirou, A comparison between BNN and regression polynomial methods for the evaluation of the effect of soiling in large scale photovoltaic plants,, Appl. Energy 108 (2011) 392–401.
[8] S.A. Kalogirou, R. Agathokleous, G. Panayiotou, On-site PV characterization and the effect of soiling on their performance, Energy 51 (2013) 439–446.
[9] S.R. Potnuru, D. Pattabiraman, S.I. Ganesan, N. Chilakapati, Positioning of PV panels for reduction in line losses and mismatch losses in PV array, Renew. Energy 78 (2015) 264–275.
[10] A. Massi Pavan, A. Mellit, D. De Pieri, V. Lughi, A study on the mismatch effect due to the use of different photovoltaic modules classes in large-scale solar parks, Prog. Photovolt. Res. Appl 22 (2014) 332–345.
[11] A. Massi Pavan, A. Tessarolo, N. Barbini, A. Mellit, V. Lughi, The effect of manufacturing mismatch on energy production for large-scale photovoltaic plants, Sol. Energy 117 (2015) 282–289.
[12] S. Djordjevic, D. Parlevliet, P. Jennings, Detectable faults on recently installed solar modules in Western Australia, Renew. Energy 67 (2014) 215–221.
[13] P. Guerriero, V. d'Alessandro, L. Petrazzuoli, G. Vallone, S. Daliento, Effective real-time performance monitoring and diagnostics of individual panels in PV plants, in: Proc. IEEE Int. Conf. Clean Electr. Power, 2013, pp. 14–19.
[14] L. Ciani, L. Cristaldi, M. Faifer, M. Lazzaroni, M. Rossi, Design and implementation of a on-board device for photovoltaic panels monitoring, in: Proc. I2MTC, 2013, pp. 1599–1604.
[15] F.J. Sánchez-Pacheco, P.J. Sotorrío-Ruiz, J.R. Heredia-Larrubia, F. Pérez-Hidalgo, M.S. De-Cardona, PLC-Based PV plants smart monitoring system: field measurements and uncertainty estimation, IEEE Trans. Instrum. Meas. 63 (2014) 2215–2222.
[16] B. Ando, S. Baglio, A. Pistorio, G.M. Tina, C. Ventura, Sentinella: smart monitoring of photovoltaic systems at panel level, IEEE Trans. Instrum. Meas. 64 (2188) (2015) 2199.
[17] T. Takashima, J. Yamaguchi, K. Otani, T. Oozeki, K. Kato, M. Ishida, Experimental studies of fault location in PV module strings, Sol. Energy Mater Sol. Cells 93 (2009) 1079–1082.
[18] L. Schirone, F.P. Califano, M. Pastena, Fault detection in a photovoltaic plant by time domain reflectometry, Prog. Photovolt. Res. App 2 (1994) 35–44.
[19] S. Vergura, G. Acciani, V. Amoruso, G. Patrono, Inferential statistics for monitoring and fault forecasting of PV plants, in: Proceedings of the IEEE International Symposium, Industrial Electronics, Cambridge, UK, 2008, pp. 2414–2419.
[20] M. Miwa, S. Yamanaka, H. Kawamura, H. Ohno, H. Kawamura, Diagnosis of a power output lowering of PV array with a (-dI/dV)-V characteristic, in: Proceeding of IEEE 4th World Conference on Photovoltaic Energy Conversion, Waikoloa, HI, 2006, pp. 2442–2445.
[21] S. Kaplanis, E. Kaplani, Energy Performance and degradation over 20 years performance of BP c-Si PV Modules, Simul. Model. Pract. Theory 19 (2011) 1201–1211.
[22] S. Silvestre, M.A. da Silva, A. Chouder, D. Guasch, E. Karatepe, New procedure for fault detection in grid connected PV systems based on the evaluation of current and voltage indicators, Energy Convers. Manag. 86 (2014) 241–249.
[23] S. Silvestre, A. Chouder, E. Karatepe, Automatic supervision and fault detection of PV systems based on power losses analysis, Energy Convers. Manag. 51 (2010) 1929–1937.
[24] W. Chine, A. Mellit, A. Massi Pavan, S.A. Kalogirou, Fault detection method for grid-connected photovoltaic plants, Renew. Energy 66 (2014) 99–110.
[25] N. Gokmen, E. Karatepe, B. Celik, S. Silvestre, Simple diagnostic approach for determining of faulted PV modules in string based PV arrays, Sol. Energy 86 (2012) 3364–3377.
[26] Y. Yagi, H. Kishi, R. Hagihara, T. Tanaka, S. Kozuma, T. Ishida, M. Waki, M. Tanaka, S. Kiyama, Diagnostic technology and an expert system for photovoltaic systems using the learning method, Sol. Energy Mat. Sol. Cells 75 (2003) 655–663.
[27] W. Yuchuan, L. Qinli, S. Yaqin, Application of BP neural network fault diagnosis in solar Photovoltaic System, in: Proceedings of the IEEE International Conference on Mechatronics and Automation, Changchun, China, 2009, pp. 9–12.
[28] S. Syafaruddin, E. Karatepe, T. Hiyama, Controlling of artificial neural network for fault diagnosis of photovoltaic array, in: Proceedings of the 16th International Conference on Intelligent System Application to Power Systems (ISAP), Greece, 2011, pp. 1–6.
[29] Z. Li, Y. Wang, D. Zhou, C. Wu, An intelligent method for fault diagnosis in photovoltaic array, ICSC Part II CCIS 327 (2012) 10–16.
[30] P. Ducange, M. Fazzolari, B. Lazzerini, F. Marcelloni, An intelligent system for detecting faults in photovoltaic fields, in: Proceedings of the 11th International Conference on Intelligent Systems Design and Applications IEEE, Cordoba, Spain, 2011, pp. 1341–1346.
[31] L. Bonsignore, M. Davarifar, A. Rabhib, G.M. Tinaa, A. Elhajjaji, Neuro-Fuzzy fault detection method for photovoltaic systems, Energy Procedia 62 (2014) 431–441.
[32] K.H. Chao, S.H. Ho, M.H. Wang, Modeling and fault diagnosis of a photovoltaic system, Electr. Power Syst. Res. 78 (2008) 97–105.
[33] Y. Zhao, L. Yang, B. Lehman, J.F. De Palma, J. Mosesian, R. Lyons, Decision-based fault detection and classification in solar photovoltaic arrays, in: Twenty Seventh Annual IEEE Applied Power Electronics Conference and Exposition, Orlando, FL, 2012, pp. 93–99.
[34] Y. Zhao, B. Lehman, J.F. De Palma, J. Mosesian, R. Lyons, Challenges to over-current protection devices under line-line faults in solar photovoltaic arrays, in: IEEE Energy Conversion Congress and Exposition (ECCE), Phoenix, Arizona, 2011, pp. 20–27.
[35] J.C. Hernandez, P.G. Vidal, A. Medina, Characterization of the insulation and leakage currents of PV generators: relevance for human safety, Renew. Energy 35 (2010) 593–601.
[36] O. Garcia, J.C. Hernandez, F. Jurado, Guidelines for Protection against Over-current in Photovoltaic Generators, Adv. Electr. Comput. Eng. 12 (2012) 63–70.
[37] J.D. Bastidas-Rodriguez, G. Petrone, A. Ramos-Paja, G. Spagnuolo, Photovoltaic modules diagnostic: an overview, in: 39th IEEE Annual Conference on Industrial Electronics Society, IECON, Vienna, 2013, pp. 96–101.
[38] W. Chine, A. Mellit, A. Massi Pavan, V. Lughi, Fault diagnosis in photovoltaic arrays, in: IEEE ICCEP, 16–18 June 2015, pp. 73–78. Sicily, (Italy).
[39] D. Sera, R. Teodorescu, P. Rodriguez, PV panel model based on datasheet values, in: Proceedings of the IEEE International Symposium on Industrial Electronics, 2007, pp. 2392–2396.
[40] J.S. Stein, C.P. Cameron, B. Bourne, A. Kimber, J. Posbic, T. Jester, A standardized approach to PV system performance model validation, in: Photovoltaic Specialists Conference (PVSC), 2010 35th IEEE, 2010, pp. 1079–1084.
[41] W. Xiao, W.G. Dunford, A. Capel, A novel modelling method for photovoltaic cells, in: Proceedings of the IEEE 35th, Annual Power Electronics Specialists Conference (PESC), 2004, pp. 1950–1956.
[42] B. Long, Détection et localisation de défauts pour un système PV, PhD thesis, University of Grenoble, 2011.
[43] BP Solar BP MSX120–120 W Multi-crystalline Photovoltaic Module Datasheet, 2002. http://www.comel.gr/.
[44] A. Mellit, S.A. Kalogirou, MPPT-based artificial intelligence techniques for photovoltaic systems and its implementation into field programmable gate array chips: Review of current status and future perspectives, Energy 70 (2014) 1–21.
[45] H. Mekki, A. Mellit, S.A. Kalogirou, A. Messai, G. Furlan, FPGA-Based implementation of a real time photovoltaic module simulator, Prog. Photovolt. Res. Appl 18 (2010) 115–127.